

# Formation depths of Fraunhofer lines

E.A. Gurtovenko, V.A. Sheminova

Main Astronomical Observatory, National Academy of Sciences of Ukraine  
Zabolotnoho 27, 03689 Kyiv, Ukraine  
E-mail: shem@mao.kiev.ua

## Abstract

We have summed up our investigations performed in 1970–1993. The main task of this paper is clearly to show processes of formation of spectral lines as well as their distinction by validity and by location. For 503 photospheric lines of various chemical elements in the wavelength range 300–1000 nm we list in Table the average formation depths of the line depression and the line emission for the line centre and on the half-width of the line, the average formation depths of the continuum emission as well as the effective widths of the layer of the line depression formation. Dependence of average depths of line depression formation on excitation potential, equivalent widths, and central line depth are demonstrated by iron lines.

## 1 Historic aspect of the problem

In the 60 years the quantitative studies of the solar atmosphere demanded knowledge of its physical characteristics at different depths. The majority of these characteristics were derived from the Fraunhofer lines observed. Naturally it was assumed that the atmospheric parameter derived from the specific Fraunhofer line must be referred to the formation depth of the line. Therefore, the question arose about the average depth of formation of spectral lines.

Recall, that the Fraunhofer line or spectral absorption line is a weakening of the intensity of continuous spectrum of radiation, resulting from deficiency of photons in a narrow frequency range, compared with the nearby frequencies. This deficiency is created by some particles that absorb the photons in the narrow frequency range (i.e. by selective absorption). The weakening of the emergent radiation at the line frequency is often called the line depression. At the solar surface for the optical depth  $\tau = 0$  the emergent line depression is defined by:

$$D_l(0) = I_c(0) - I_l(0), \quad (1)$$

where  $I_l(0)$  is the intensity of the emergent line emission,  $I_c(0)$  is the intensity of the continuous emission at the frequency considered in the case if this line would be absent.

In the 60 years in Kiev we also began to study of the structure and dynamics of the solar atmosphere. We believed that the line formation depth is determined by the contribution function (CF) to the emergent line emission  $I_l$ . It is easily calculated. The

solution of the transfer equation for the optical depth  $\tau = 0$  gives an expression for the emergent intensity at the line frequency:

$$I_l(0) = \int_0^{\infty} S \exp(-\tau/\mu) d\tau/\mu, \quad (2)$$

where  $\tau = \tau_l + \tau_c$  is the total (line + continuum) optical depth. Here and further in the text the subscript  $l$  means the quantity refers to the line and  $c$  to the continuum.  $S$  is the total source function, and  $\mu = \cos\theta$  is the cosine of the angle between the direction of the radiation and the normal to the surface. For simplicity we have adopted  $\mu = 1$  in the subsequent formulas. Taking into account the following relationships

$$S = \frac{S_c + \eta S_l}{1 + \eta}, \quad \eta = \frac{\kappa_l}{\kappa_c}, \quad d\tau = (1 + \eta) d\tau_c, \quad (3)$$

one can write the equation (2) in the scale of integration  $\tau_c$ :

$$I_l(0) = \int_0^{\infty} (S_c + \eta S_l) \exp(-(\tau_l + \tau_c)) d\tau_c = \int_0^{\infty} F_E d\tau_c. \quad (4)$$

Here,  $\kappa_c$ ,  $\kappa_l$  are the coefficients of the continuous and selective absorption,  $F_E$  is the contribution function to emergent line emission or *the emission CF*. It presents the contributions from atmospheric layers located between  $\tau_c$  and  $\tau_c + d\tau_c$  to the intensity of the emission observed in the line frequency. The emergent intensity of the nearby continuum at the frequency considered is defined by following formula:

$$I_c(0) = \int_0^{\infty} S_c \exp(-\tau_c) d\tau_c = \int_0^{\infty} F_C d\tau_c, \quad (5)$$

where  $F_C$  is the contribution function to emergent continuous emission.

The application of the emission CF for calculation of the average depth of formation of the absorption line in our practice has convinced us that this is wrong. The average depths obtained are practically identical for all very weak lines with different excitation potentials at the similar wavelength. At that time it was well known that the very weak lines with higher excitation potentials are formed in the deeper layers of the photosphere compared with the similar lines with lower excitation potentials. We were forced to find a new method for determining the average depth of formation of spectral line.

In the 70 years, we began a detailed study of this problem together with well-known astrophysicist C. de Jager [12]. We showed that it is important to distinguish the formation regions of the line emission and line depression. They may be different. Also we showed that it should use the depression contribution function based on the Unsold's weighting function to determine the average depth of formation of the line depression. We used the weighting function under LTE conditions which was written as:

$$g'(\tau_c) = \int_{\tau_c}^{\infty} B \exp(-\tau_c) d\tau_c - B \exp(-\tau_c). \quad (6)$$

Here,  $g'$  is differently defined than the customary weighting function  $g$  derived by Unsold [33]. By multiplying the Unsold's weighting function  $g$  with  $I_c(0)$ , we has obtained  $g'$ .

With the function  $g'$  the expression for the emergent line depression in the intensity units has the following form:

$$D_l(0) = \int_0^{\infty} g' \eta \exp(-\tau_l) d\tau_c = \int_0^{\infty} F_D d\tau_c. \quad (7)$$

Here,  $F_D$  is *the depression CF*. If the absorbing particles are absent ( $\kappa_l = 0$ ,  $\eta = 0$ , and  $F_D = 0$ ), the contributions to the line depression equal zero. One can divide (7) by  $I_c(0)$  to obtain the expression for the relative depression ( $R_l(0) = D_l(0)/I_c(0)$ ) and the contribution function to the relative depression ( $F_R = F_D/I_c(0)$ ). The function  $F_R$  corresponds to the contribution function derived by Unsold [33] and Pecker [25].

In our next paper [11] we calculated the average depths of formation for many weak spectral lines using the function  $F_D$ . The obtained depths of formation of weak lines showed a clear dependence on the excitation potential. Thus, we confirmed the validity of the determination of the average formation depth with the contribution function  $F_D$  as well as  $F_R$ .

After the our papers [11, 12], a lot of other papers devoted to this problem have appeared. The opinions of the authors of the papers were strongly divided. Some authors (e.g., Demidov [5, 6]) supported our concept of the depression CF. Other authors (Babiy and Rykalyuk [2], Buslavsky [4], Lyubimkov [21], and etc.) defended the concept of the emission CF from more great tenacity. Third authors (Makita [23], Beckers and Milkey [3], and etc.) have proposed new methods of calculating the formation depth of absorption line. There were objective reasons to explain why our concept was not immediately accepted and the problem of the formation depths was discussed for a long time. We can call the main reasons.

1. The inertia of thinking. Having solved the problem of radiative transfer in the atmosphere of the Sun and stars, classical astrophysics determined the line formation depth by the simple way. The first definition was based on the emergent line emission. Minnaert [24] assumed the average depth of formation of absorption line is equal to the depth which divides the  $F_E$ -curve in to equal halves. The second definition was based on the approximation that the emergent line intensity is equal to the source function at the average line formation depth  $\langle\tau_c\rangle$ . Under the LTE conditions this is

$$I_l(0) = B(\langle\tau_c\rangle). \quad (8)$$

Using a photospheric model or data on the centre-to-limb variation of the absolute continuum  $I_c$ , one can easily obtain  $\langle\tau_c\rangle$ . If the Plank function  $B$  varies linearly with  $\tau_c$  one can use the important Eddington-Barbier approximation  $I_l(0) = B(\tau_c = \mu)$ . Since then, many astrophysics automatically use the solution of the transfer equation for the emergent line intensity  $I_l$  to determine the average depth of formation of spectral line with the help of the emission CF (although it was fundamentally wrong).

2. In the 70s and 80s the astrophysics did not take into account the results of earlier works on this issue. In the 50–60s Minnaert [24] and de Jager [20] did not regard the emission CF for determination of the average depth of formation of the Fraunhofer line. While Elste [7] and Ruhm [26] have pointed to the need to use the Unsold-Pecker CF.

3. The Unsold-Pecker CF was derived by mathematical transformation to simplify the description of the Fraunhofer lines. Unsold [33] and later Pecker [25] did not explain the physical meaning of the function  $F_R$ . Apparently, in our first paper [12] the physical sense of the function  $F_D$  was not convincingly substantiated. It was masked by the fact that

we used the LTE condition ( $S_c = S_l = B(T)$ ). If LTE is absent the weighting function

$$g'(\tau_c) = \int_{\tau_c}^{\infty} S_c \exp(-\tau_c) d\tau_c - S_l \exp(-\tau_c). \quad (9)$$

At that rate it is evident that the left term of (9) the multiplied by  $\eta \exp(-\tau_l)$  presents the contribution to the absorption by selectively absorbing particles at the depth  $\tau_c$ , while the right term (with negative sign) multiplied by  $\eta \exp(-\tau_l)$  presents the contribution to the re-emission by selectively absorbing particles. Such explanation was absent in our first article [12], and this is also not facilitate the timely approval of our concept.

Due to the current confusing situation, we published a series of new papers [13]–[18] and [29]–[31]. It should note, at the same time Sarychev [28] supported the concept of the depression CF and actively cooperated with us. Magain [22] presented the correct solution of the transfer equation for the relative line depression  $R_l(0)$  and obtained the rigorous expression for the CF to the relative line depression. Gurtovenko and Sarychev [14] have shown that the depression CF obtained by Magain is identical to the Unzold-Pecker CF.

By the end of 80 years, we were convinced that the problem of the formation depths of spectral lines has already been solved. Nevertheless, a series of new papers have appeared. Achmad [1] raise the issue again and proposed a new method which confirms the correctness of our concept. Grossmann-Doerth et al. [9], Ruiz Cobo and Toro Inesta [27], and Staude [32] developed the concept of depression functions for four Stokes profiles of the absorption lines.

The purpose of this paper to summarize the results of our researches on this issue, to demonstrate the features of the different contribution functions for different lines and to show the localization of the absorption and emission processes involved in the formation of the lines. Furthermore, we want to demonstrate the average depth of formation of different lines in solar spectrum. The lines selected by us are often used in the interpretation of many phenomena in the solar atmosphere, therefore the knowledge of the average depths of formation of emission and depression of these lines can be useful for astrophysics.

## 2 Formation of absorption line

The physical sense of the depression contribution function becomes perfectly clear, when we examine the specific processes forming a absorption line. It is well known that absorption line originates as a consequence of a chain of absorption and emission processes caused by the presence selectively absorbing particles in the photospheric layers. Fig. 1 demonstrates a schematic ratio of the quantities that characterizes the processes forming the Fraunhofer line. Let's look these processes separately from each other and present them quantitatively by the physical approach.

1. **Selective absorption.** If we assume that selectively absorbing particles only absorb, the processes of selective re-radiation are absent, i.e.,  $\epsilon_l = 0$  and  $S_l = 0$ , then the portion of radiation absorbed selectively at the depth  $z$  within an elementary layer  $\Delta z$  at the line frequency will equal to

$$\Delta D_l^p(z) = I_c(z) \exp(-\tau_l(z)) \exp(-\tau_c(z)) \kappa_l(z) \Delta z. \quad (10)$$

Here  $\exp(-\tau_l(z)) \exp(-\tau_c(z))$  is the factor of the radiation attenuation by the selective absorbing particles and continuous absorption. After substitution of the expression for

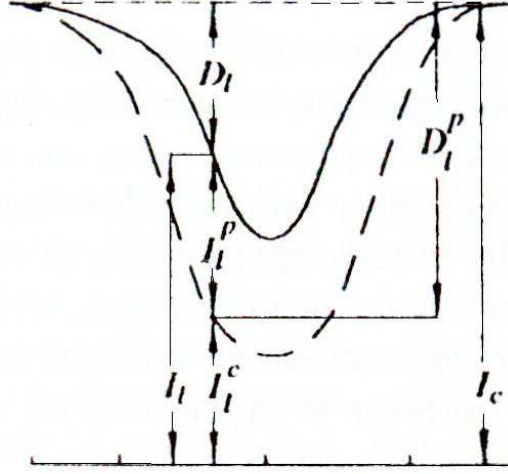


Figure 1: The quantities of the contributions to observed profile of a Fraunhofer line (solid line) connected with the emission and depression processes forming the line and continuum. The intensity of observed line emission  $I_l = I_l^c + I_l^p$ . The observed profile of emergent line depression  $D_l = D_l^p - I_l^p$ . While  $I_c$  is the intensity of the nearby continuum. If the selective absorbing particles did not produce the proper emission ( $I_l^p = 0$ ), the observed line would have the profile shown by a dashed line

the intensity of continuous radiation coming from the level  $\tau_c$

$$I_c(\tau_c) = \exp(\tau_c) \int_{\tau_c}^{\infty} S_c(\tau_c) \exp(-\tau_c) d\tau_c, \quad (11)$$

and integration in the  $\tau_c$  scale, we obtain the expression for amount of the radiation absorbed selectively for  $\tau_c = 0$ :

$$D_l^p(0) = \int_0^{\infty} \left[ \int_{\tau_c}^{\infty} S_c(\tau_c) \exp(-\tau_c) d\tau_c \right] \exp(-\tau_l) \eta d\tau_c. \quad (12)$$

We call the quantity  $D_l^p$  as *the proper line depression*.

**2. Selective re-emission.** Under real conditions  $\epsilon_l \neq 0$  and  $S_l \neq 0$ . Some portion of the proper line depression is be re-radiated in the line frequency. We call it as *the proper line emission*. Analogously to (10), the intensity of proper line emission equals:

$$\Delta I_l^p(z) = \epsilon_l(z) \exp(-\tau_l(z)) \exp(-\tau_c(z)) \Delta z. \quad (13)$$

Taking into account  $\epsilon_l = S_l \kappa_l = S_l \kappa_c \eta$  and integrating over  $\tau_c$ , we obtain the analytical expression for the emergent intensity of proper line emission at the surface for the frequency within a spectral line:

$$I_l^p(0) = \int_0^{\infty} S_l \exp(-(\tau_c + \tau_l)) \eta d\tau_c. \quad (14)$$

**3. Continuous emission at the frequency within the spectral line.** The selectively absorbing particles are not completely "eat" the continuous radiation coming out

in the line frequency. Some part of the radiation comes out. We call it as *the continuous emission passed through the line*. The analytical expression for the intensity of the continuous emission passed through the line can be obtained by the same simple way:

$$\Delta I_l^c(z) = \epsilon_c(z) \exp(-\tau_l(z)) \exp(-\tau_c(z)) \Delta z. \quad (15)$$

After substitution of  $\epsilon_c = S_c \kappa_c$  and integration over  $\tau_c$ , we obtain:

$$I_l^c(0) = \int_0^\infty S_c \exp(-(\tau_c + \tau_l)) d\tau_c. \quad (16)$$

4. **Emergent line emission** is the sum of the proper line emission and the continuous emission passed through the line:

$$I_l(0) = I_l^p(0) + I_l^c(0) = \int_0^\infty (S_c + \eta S_l) \exp(-(\tau_c + \tau_l)) d\tau_c. \quad (17)$$

The integrand in (17) is the emission contribution function  $F_E$  (4) derived from the solution of the transfer equation for the emergent line intensity.

5. **Observed line depression** is also formed by two processes. The first process forms the proper line depression and the second forms the proper line emission. The physical sum (or the mathematical difference) of the intensities of the proper depression and emission at the line frequency gives the expression for the *observed line depression*:

$$D_l(0) = D_c^p(0) - I_l^p(0) = \int_0^\infty \left[ \int_{\tau_c}^\infty S_c \exp(-\tau_c) d\tau_c - S_l \exp(-\tau_c) \right] \eta \exp(-\tau_l) d\tau_c. \quad (18)$$

The integrand in (18) is the depression CF. Under the LTE approximation it corresponds to the expression  $F_D$  (7) derived with the help of the weighting functions  $g'$ .

### 3 Features of the contribution functions

In the spectral analysis one can use the emission and depression CFs as well as the CFs to proper line emission and proper line depression. All the CFs carry the valuable information. The information on an amount and location of the proper line emission, proper line depression, or the continuous emission passed by the line has great practical significance in the study of the relationship between the observed phenomena, parameters of the solar atmosphere, and spectral lines. For example, the brightness contrasts observed in different lines are compared with such phenomena as concentration of magnetic field. To study such phenomena we must use the CF to the proper line emission  $I_l^p$ , while to study the photospheric velocity fields derived from the Doppler lineshifts we should use the depression CF to  $D_l$ .

We calculated the CFs under LTE conditions with photospheric model HOLMU for the center of different lines at the solar disc center in logarithmic scale of optical depths  $\log \tau_5$ . The scale  $\log \tau_5$  is more convenient to analyze spectral lines in stellar atmospheres. Figs 2–4 are shown the CFs calculated. Specific CF at specific  $\log \tau_5$  shows the contribution of the layer situated at this depth to the quantity by the specific process.

The emergent intensity of continuum ( $I_c$ ) is effectively formed in the deepest layers of the photosphere. The formation region of the intensity of continuous emission passed

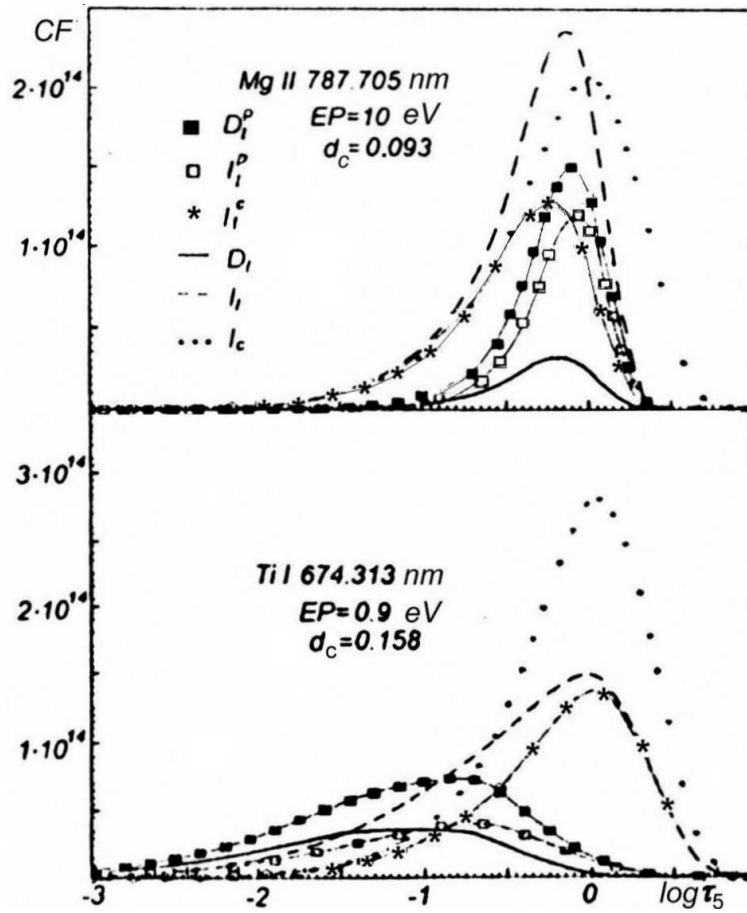


Figure 2: Contribution functions to the quantities  $D_l^p$ ,  $I_l^p$ ,  $I_l^c$ ,  $D_l$ ,  $I_l$ ,  $I_c$  at the center of weak Fraunhofer lines

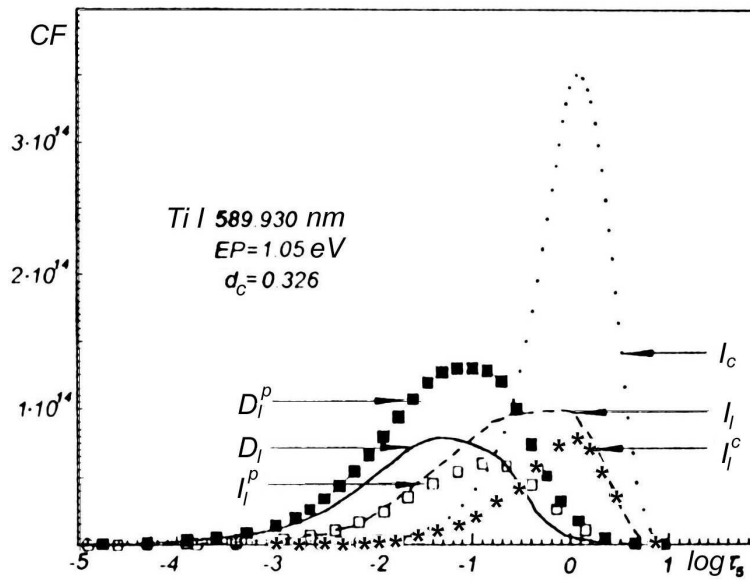


Figure 3: The contribution functions at the center of a moderate Fraunhofer line

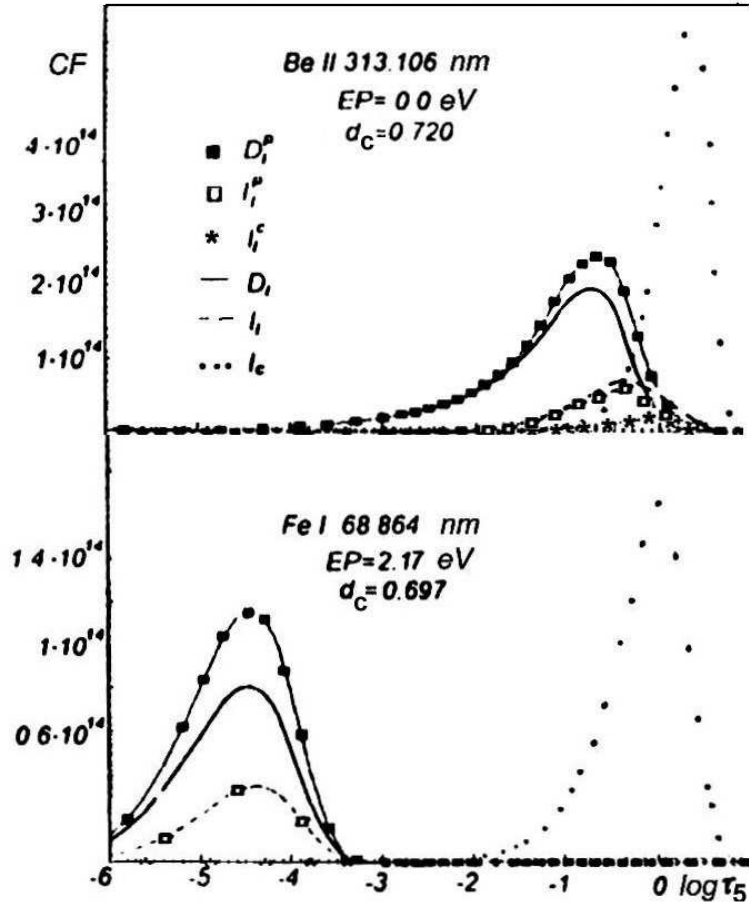


Figure 4: The contribution functions at the center of strong Fraunhofer lines

through the line ( $I_l^c$ ) is always located within the region of formation of the nearby continuum. While the formation regions of the proper line depression ( $D_l^p$ ) the proper line emission ( $I_l^p$ ) as well as the line depression ( $D_l$ ) are not associated with the formation of the continuum. They are always associated with the location of selectively absorbing particles. Therefore the effective contributions to  $D_l^p$ ,  $I_l^p$ , and  $D_l$ , are formed in the same layers slightly offset from each other. The CF to the emergent line intensity,  $I_l$ , may in principle have two peaks, since it includes the contributions associated with selective re-emission and the continuum emission passed through the line. Fig. 3 demonstrates the contributions to  $I_l^p$  and  $I_l^c$  that are formed in different layers in the case of a moderate line, while in the case of the very weak line (Fig. 2, Mg II 787.705 nm) they are formed practically in the same layers. The magnitude and location of the maximum of the CFs basically depends on the line strength, but they also depend on other line parameters. Let's consider the CFs calculated for the weak, moderate, and strong lines, separately.

*Weak lines.* Figure 2 shows the CFs calculated for very weak line of Mg II (787.705 nm). Due to small optical thickness in very weak line its CF clearly indicates the location of the region of effective formation of the line. Another important feature is that the very weak line is formed very deeply in the photosphere. The greater the excitation potential, the deeper and narrower the line formation region. Important feature of the very weak lines with very high EP is a large amount of the proper line emission  $I_l^p$  and the proper line depression  $D_l^p$  compared with the observed line depression  $D_l$ . Large amount of the proper line emission is remarkable feature to explore of the solar and stellar atmospheres.

The weak lines with low excitation potentials also draw attention to themselves. For



example, the Ti I 674.313 line (Fig. 2) has the proper line emission  $I_l^p$  is comparable to the observed line depression  $D_l$ . It is interesting that for this line the location of the line emission differs significantly from the formation region of the line depression. For weak lines with high excitation potentials the difference is much smaller. The formation region of resonance weak lines is located slightly higher than usual weak lines with low excitation potentials, while weak lines of molecules are formed within the highest layers of the photosphere [28].

*Moderate lines.* As we can see in Fig. 3, the formation regions of the proper line emission, the proper line depression, and observed line depression in the case of moderate lines are shifted to higher layers of the photosphere as compared with weak lines with the same excitation potentials and wavelengths. A known fact of the decrease of the depth of formation region of the moderate lines in comparison with the weak lines is confirmed. For moderate line the amount of the continuum emission passed through the line is clearly reduced. The dependence of formation depth of moderate line on the excitation potential is the same as that for weak lines.

*Strong lines.* It is known, that there is no any strong lines with high excitation potentials in the solar spectrum, which could be formed in the deep layers of the photosphere. Figure 4 shows the CFs calculated for strong lines with low excitation potentials. We found only one resonance line (313.106 Be II), which is formed in the deep layers. Partly, it is a consequence of its short wavelength. This line passes a small portion of the continuum emission, whereas the other strong lines practically do not transmit continuous radiation outwards. Therefore, the emergent line intensity  $I_l$  of strong lines usually equals the intensity of the proper line emission  $I_l^p$ . Its amount is significantly smaller compared with the observed line depression  $D_l$  or the proper line depression  $D_l^p$ . Thus, the small value of the observed central intensity  $I_l$  in the strong lines is determined only by its proper emission re-emitted by the selectively absorbing particles. Hence it becomes clear why the average depths of formation of emergent line emission and line depression are the same in the strong lines. Fig. 4 also shows the CFs for strong atypical chromospheric line (868.864 nm Fe I), which is formed in the uppermost layers of the photosphere or practically in the low chromosphere. The location of the region of effective formation of the strong line depends mainly on the line strength.

We did not consider the strongest line, since their central part is formed in the absence of the LTE conditions. Under non-LTE, the relation between the population of the upper and lower levels deviates dramatically from LTE equilibrium and can be quite different at different depth in the photosphere. The shape and magnitude of the CFs to  $D_l^p$ ,  $I_l^p$ ,  $D_l$  can significantly change. In the case if the proper line emission  $I_l^p$  is very strong and the line depression  $D_l$  is negative, then the emission appears at the line center. Such phenomenon can occur in the spectrum of the solar flares as the appearance of the emission lines on the background of the continuum.

## 4 The average depth of formation of a spectral line

Despite the fact that nowadays every researcher has a computer and one can calculate the average depth of formation of any line, and despite the fact that Gurtovenko and Kostyk [10] have published the mean geometrical depths of formation of the line center for 1958 Fraunhofer lines of different elements, we decided to present in accessible form more complete information about the average depths of the 503 reference spectral lines. These lines can serve as probes to diagnose the physical conditions of the various layers

in the photosphere.

Since the depression contribution function  $F_D$  (7) determines the weight of the relevant layers in contributing to the emergent line depression, one may define a average depth of formation of the line at a given wavelength profile point ( $\lambda$ ) at a position  $\mu$  on the solar (stellar) disk by the following formula:

$$\langle x \rangle_\mu = \int_{-\infty}^{\infty} x F_D(x, \mu) dx / \int_{-\infty}^{\infty} F_D(x, \mu) dx. \quad (19)$$

Here,  $x$  can be equal to  $\tau_5$ ,  $\log \tau_5$  or  $z$ . The effective depth of formation of the entire line profile at the position  $\mu$  is determined by averaging over the whole profile:

$$\langle x \rangle_{\mu, \text{eff}} = \int_{\lambda_1}^{\lambda_2} \langle x \rangle_\mu R(\lambda, \mu) d\lambda / \int_{\lambda_1}^{\lambda_2} R(\lambda, \mu) d\lambda, \quad (20)$$

where  $R(\lambda, \mu)$  is the relative line depression at the profile point  $\lambda$  and at the position  $\mu$ , and  $\lambda_1$ ,  $\lambda_2$  are initial and final wavelength points of the line profile.

Averaging over the solar disk one can obtain the mean depth of formation of the line depression at a given profile point  $\lambda$  for the Sun as a star (or for any star):

$$\langle x \rangle^* = \int_0^1 \langle x \rangle_\mu \mu d\mu, \quad (21)$$

and the effective formation depth of the entire line profile for the Sun as a star:

$$\langle x \rangle_{\text{eff}}^* = \int_{\lambda_1}^{\lambda_2} \langle x \rangle^* R^*(\lambda) d\lambda / \int_{\lambda_1}^{\lambda_2} R^*(\lambda, \mu) d\lambda, \quad (22)$$

where the superscript  $*$  means the quantity averaged over the solar (stellar) disk.

Analogously, one can compute the mean depth for the emergent line emission using the emission contribution function  $F_E$  (4) in (19–22). The mean depth of formation the nearby continuum for each line one can compute using the CF to continuum  $F_C$  (5). The CFs to line depression, line emission, and continuum do not change sing, therefore the formulas (19–22) give reliable results.

The effective width of the region of formation of line depression at the line center and the center of the solar disk ( $\mu = 1$ ) one can define as:

$$\Delta x_{\text{eff}} = \int_{-\infty}^{\infty} (x - \langle x \rangle)^2 F_D(x) dx / \int_{-\infty}^{\infty} F_D(x) dx, \quad (23)$$

where  $\langle x \rangle$  is the average depth of formation of the line depression at the line center. Thus,  $\Delta x_{\text{eff}}$  is the width of the layer in which occurs the main part of all contributions to the observed line depression at the line center.

Our calculations of the CFs and the average depth of formation of the lines were performed with a software package SPANSAT [8], the solar photosphere model HOLMU [19], the microturbulent velocity  $\xi_{\text{mic}} = 0.95$  km/s, the macroturbulent velocity  $\xi_{\text{mac}} = 1.75$  km/s, and the damping constant  $1.5\gamma_{\text{wdw}}$ . The abundance of chemical elements and line oscillator strengths ( $A_{gf}$ ) were determined in the process of calculation by comparing

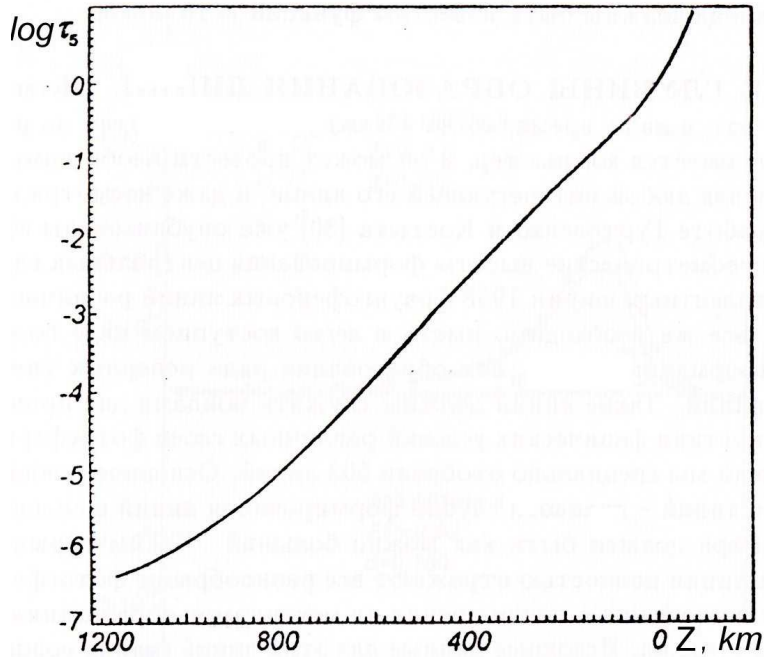


Figure 5: The optical depth as a function of the geometrical depth (HOLMU model)

the observed and calculated central depths of lines. The line parameters: wavelength  $\lambda$ , excitation potential EP, and observed central line depth  $d = (I_c - I_l)/I_c$  were taken from the tables of Gurtovenko and Kostyk [10]. The results obtained are presented in a Table. It lists the parameters of the Fraunhofer lines and the average depths of formation of line depression and line emission calculated at the centre and half-width of line profile as well as the nearby continuum. All calculations are performed at the centre of solar disk. The average depths calculated are given in the scale  $\log \tau_5$ . To convert the optical depth to the geometrical depth, we present the dependence of the optical depth  $\log \tau_5$  on geometrical depth  $z$  in Fig. 5. The effective width is given in the geometrical depth.

On the average, the depth of formation of the continuum equals  $\log \tau_5 \approx 0$ . It slightly depends on the wavelength due to the nonlinear wavelength dependence of the absorption coefficients. The average depth of formation of the continuum changes from  $\log \tau_5 = 0.163$  to 0.001 in the wavelength range from 400.0 to 520.0 nm and from  $\log \tau_5 = 0.001$  to  $-0.215$  in the wavelength range from 520.0 to 900.0 nm. This effect is easy to trace in Figs 2–4.

The average depth of formation of the very weak line may be even greater than the average depth of formation of the nearby continuum. We found the 597.88 Si II line with EP = 10.07 eV and  $\langle \log \tau_5 \rangle = -0.062$ , while the nearby continuum has  $\langle \log \tau_5 \rangle = -0.088$ . This is not a paradox, but a natural feature of very weak lines with high EP. The far wings of specific very strong lines are also formed in the deepest layers of the photosphere (e.g., the H and K Ca II lines).

In the Table there are few strong lines which are formed in the region of temperature minimum. This is the 455.40 Ba II line ( $\langle \log \tau_5 \rangle = -5.757$ ), the 649.69 Ba II line ( $\langle \log \tau_5 \rangle = -4.915$ ), the 868.86 Fe I line ( $\langle \log \tau_5 \rangle = -4.826$ ), and the 832.70 Fe I line ( $\langle \log \tau_5 \rangle = -4.293$ ). A lot of lines with  $\langle \log \tau_5 \rangle = -3$  to  $-4$  are formed in the upper photosphere, but the vast majority of lines with  $\langle \log \tau_5 \rangle = -0.5$  to  $-2$  are formed in the middle of the photosphere.

Figs 6–8 demonstrate the average depth of formation of the center of iron lines depending on the excitation potential EP, equivalent width  $W$ , and the relative depression

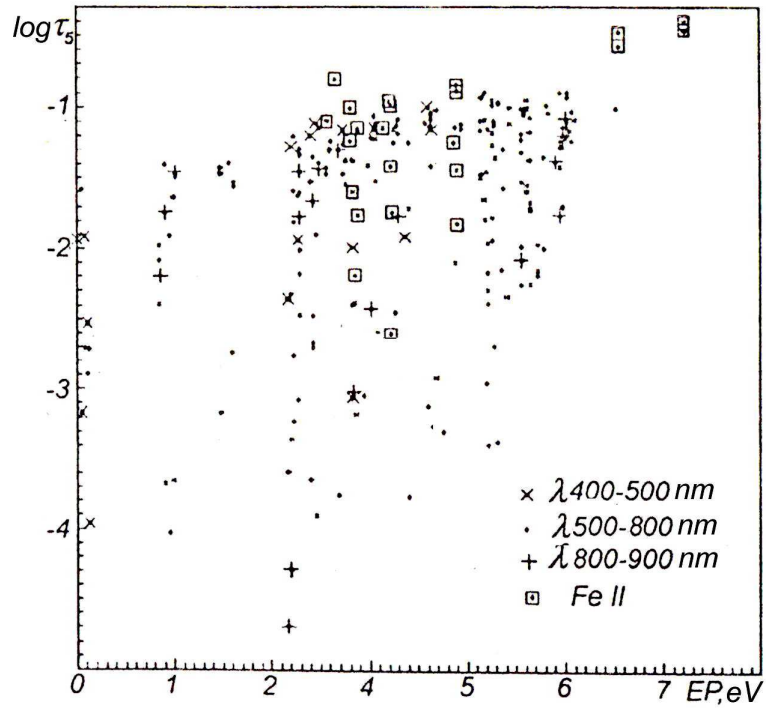


Figure 6: The average depth of line formation  $\log \tau_5$  vs. the potential excitation  $EP$  for iron lines. The data for Fe II lines are marked by squares, while the data for the Fe I line are marked by the other icons. Large scatter of the values of formation depths is caused the difference in the line parameters, such as the wavelength and central line depth

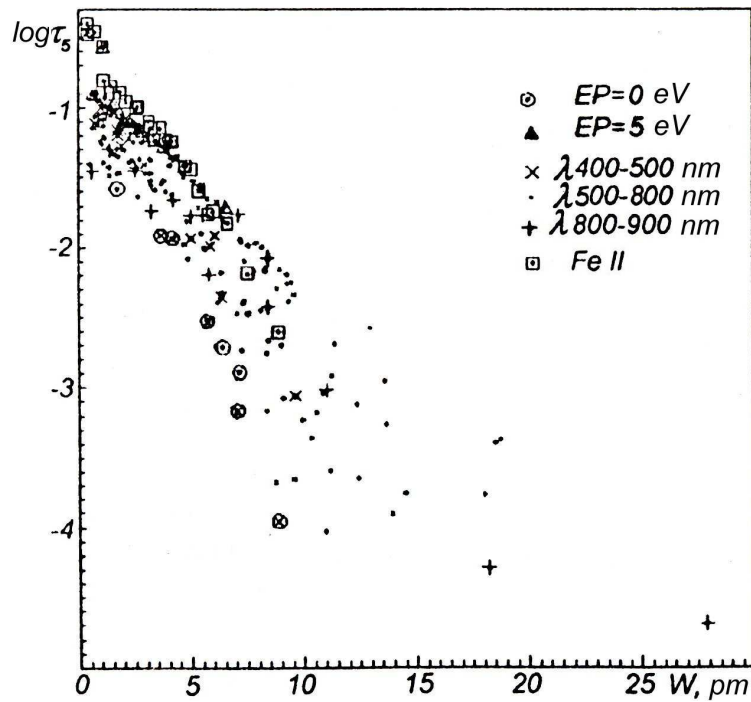


Figure 7: The average depth of line formation  $\log \tau_5$  vs. equivalent width  $W$

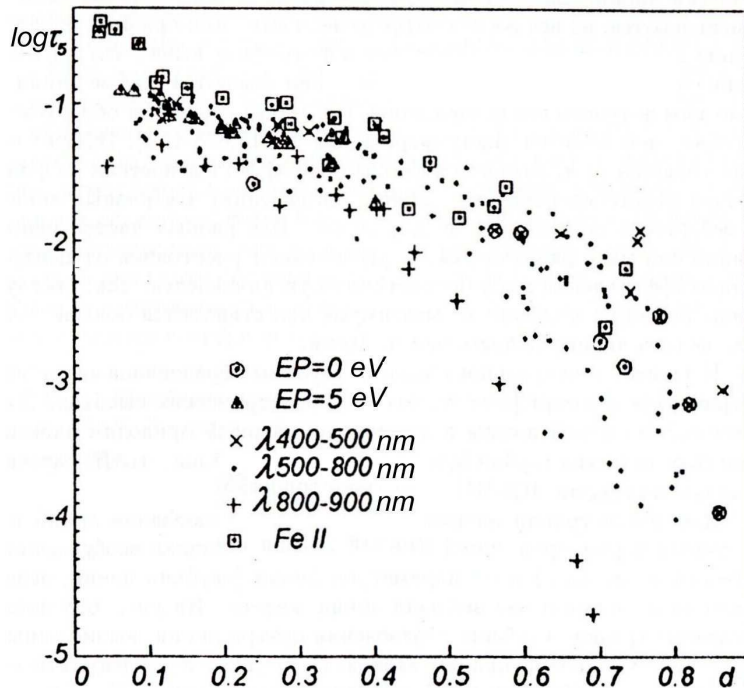


Figure 8: The average depth of line formation  $\log \tau_5$  vs. central line depth  $d$

at the line center  $d$  (or central line depth.) With the help of these Figures it is possible to estimate the average depth of iron lines, which are absent in our Table.

Note also that the effective widths  $\Delta z_{\text{eff}}$  calculated for different Fraunhofer lines differ from each other. They vary in the range 50–120 km from one line to another, while the differences from one point to another within the line profile is sufficiently small ( $\approx 10$  km).

## 5 Conclusion

We have demonstrated that line emission and line depression contribution functions are different in their essence. The emission function defines the contributions of elementary photospheric layers to the emergent continuous emission and selective re-emission at the line frequency, whereas the depression function defines the contributions of these layers to the observed selective depression and selective re-emission at the frequency considered. If selectively absorbing particles are absent in the photospheric layers, the depression function is equal to zero, while the emission function is not zero. The depression contribution function characterizes the magnitude of deficit of the emerging radiation at the line frequency relatively the continuum level, i.e, it characterizes the magnitude of Fraunhofer line. To correctly calculate the average depth of formation of the Fraunhofer line you should use the depression contribution function derived through the weighting function.

We examined in detail the physical processes involved in the formation of the spectral line. The understanding of these processes is useful not only for the study of such phenomena as Fraunhofer lines, but also for the correct selection of lines to study of specific events in the solar atmosphere.

Sheminova V.A. is sincerely grateful to A.S. Gadun, R.I. Kostyk, M.Ya. Orlov for useful advice and valuable comments.

## References

- [1] Achmad L. 1992, *Solar Phys.*, 138, 411
- [2] Babij B. T., Rykalyuk R. E. 1981, *Astron. Zh.*, 58, 825
- [3] Beckers J. M., Milkey R. W. 1975, *Solar Phys.*, 43, 289
- [4] Buslavsky V. G. 1969, *Izv. Krymskoj Astrofiz. Obs.*, 39, 317
- [5] Demidov M. L. 1980, *Iss. Geomag. Aeron. i Fiz. Sol.*, 52, 3
- [6] Demidov M. L. 1983, *Iss. Geomag. Aeron. i Fiz. Sol.*, 65, 37
- [7] Elste G. 1955, *Z. Astrophys.*, 37, 201
- [8] Gadun A. S., Sheminova V. A. SPANSAT: the Program for LTE Calculations of Absorption Line Profiles in Stellar Atmospheres, 1988, Preprint of Inst. Theor. Phys. AS USSR, ITF-88-87P, Kiev., 37p.
- [9] Grossmann-Doerth U., Larsson B., Solanki S. K. 1988, *Astron. and Astroph.*, 204, 266
- [10] Gurtovenko E. A., Kostyk R. I., Fraunhofer spectrum and a system of solar oscillator strengths, 1989, Kiev, Izdatel'stvo Naukova Dumka, 200p.
- [11] Gurtovenko E. A., Ratnikova V. A. 1974, *Astron. Zh.*, 51, 1032
- [12] Gurtovenko E. A., Ratnikova V. A., de Jager C. 1974, *Solar Phys.*, 37, 43
- [13] Gurtovenko E. A., Ratnikova-Sheminova V. A. 1978, *Solar Phys.*, 58, 241
- [14] Gurtovenko E. A., Sarychev A. P. 1988, *Astron. Zh.*, 65, 653
- [15] Gurtovenko E. A., Sheminova V. A. 1983, *Astron. Zh.*, 60, 982
- [16] Gurtovenko E. A., Sheminova V. A. 1985, *Astron. Zh.*, 62, 988
- [17] Gurtovenko E. A., Sheminova V. A. 1985, *Byull. Sol. Dannye AN USSR*, 1, 70.
- [18] Gurtovenko E. A., Sheminova V. A., Sarychev A. P. 1991, *Solar Phys.*, 136, 239
- [19] Holweger H., Mueller E. A. 1974, *Sol. Phys.*, 39, 19
- [20] Jager C. de The Hydrogen Spectrum of the Sun, 1952, Thesis, Utrecht, Rech. Astron. Obs.. Utrecht. V. XIII (1)
- [21] Liubimkov L. S. 1976, *Krym. Astrof. Obs., Izv.*, 55, 164
- [22] Magain P. 1986, *Astron. and Astrophys.*, 163, 135
- [23] Makita M. 1977, *Solar Phys.*, 51, 43
- [24] Minnaert M. 1948, *Bull. Astron. Inst. Neth.*, 10, 399
- [25] Pecker J.-C. 1951, *Ann. Astrophys.*, 14, 115

- [26] Ruhm H. 1969, *Astron. and Astrophys.*, 3, 277
- [27] Ruiz Cobo B., del Toro Iniesta J. C. 1994, *Astron. and Astrophys.*, 283, 129
- [28] Sarychev A. P. 1986, *Soviet Astronomy*, 30, no.3, 329
- [29] Sheminova V. A. 1992, *Kinem. i Fiz. Neb. Tel*, 8, no. 3, 44
- [30] Sheminova V. A., Gurtovenko E. A. 1978, *Astrom. i Astrof.*, 36, 21
- [31] Sheminova V. A., Gurtovenko, E. A. 1978, *Astrom. i Astrof.*, 36, 32
- [32] Staude J. 1996, *Solar Phys.*, 164, 183
- [33] Unsold A. 1932, *Z. Astrophys.*, 4, 339

**Table.** Select spectral lines: wavelengths ( $\lambda$ ); excitation potentials of the lower level (EP); central line depths ( $d$ ); effective widths of the line formation region ( $\Delta z_{\text{eff}}$ ); average formation depths ( $\langle \log \tau_5 \rangle$ ) of emergent line emission  $I_l$  and depression  $D_l$  at the line center; emergent line emission and depression at the line half-width  $D_l/2$ ; average depth of formation of the nearby continuum  $I_c$ . The average depths were calculated for the spectral lines at the center of the solar disc.

$\lambda$ (nm)	Element	EP (eV)	$d$	$\Delta z_{\text{eff}}$ (km)	$I_l$	$D_l$	$\langle \log \tau_5 \rangle$ $I_l/2$	$D_l/2$	$I_c$
670.77	Li I	0.00	.010	109	-0.147	-1.180	-0.146	-1.132	-0.144
313.10	Be II	0.00	.720	129	-0.193	-1.238	0.098	-0.772	0.181
481.73	C I	7.48	.138	60	-0.139	-0.253	-0.051	-0.139	0.047
505.21	C I	7.68	.252	63	-0.361	-0.411	-0.180	-0.207	0.015
538.03	C I	7.68	.158	62	-0.274	-0.337	-0.157	-0.193	-0.025
658.76	C I	8.53	.083	59	-0.307	-0.299	-0.230	-0.179	-0.136
711.31	C I	8.64	.118	60	-0.430	-0.395	-0.314	-0.236	-0.169
833.51	C I	7.68	.355	78	-1.084	-1.095	-0.638	-0.547	-0.206
960.30	C I	7.48	.280	77	-0.936	-0.942	-0.585	-0.523	-0.215
868.33	N I	10.33	.041	48	-0.354	-0.179	-0.292	-0.080	-0.212
939.28	N I	10.69	.050	46	-0.397	-0.204	-0.319	-0.089	-0.216
615.67	O I	10.74	.039	42	-0.203	-0.053	-0.160	0.032	-0.104
615.81	O I	10.74	.028	42	-0.180	-0.028	-0.147	0.048	-0.104
630.03	O I	0.00	.038	134	-0.128	-1.264	-0.122	-1.199	-0.115
777.53	O I	9.14	.249	63	-0.789	-0.690	-0.524	-0.380	-0.199
475.18	Na I	2.10	.128	98	0.008	-0.872	0.029	-0.727	0.057
615.42	Na I	2.10	.289	100	-0.372	-1.105	-0.219	-0.874	-0.104
616.07	Na I	2.10	.428	100	-0.673	-1.313	-0.297	-0.907	-0.104
996.12	Na I	3.62	.036	96	-0.241	-0.952	-0.231	-0.732	-0.211
473.00	Mg I	4.34	.534	101	-0.442	-1.244	-0.104	-0.809	0.060
571.10	Mg I	4.34	.678	91	-1.814	-2.121	-0.423	-0.882	-0.061
631.92	Mg I	5.11	.192	98	-0.277	-0.977	-0.198	-0.785	-0.117
765.76	Mg I	5.11	.496	92	-1.488	-1.805	-0.577	-0.917	-0.194
847.36	Mg I	5.93	.054	96	-0.249	-0.971	-0.235	-0.748	-0.209
871.77	Mg I	5.93	.323	97	-0.766	-1.313	-0.470	-0.795	-0.213
892.35	Mg I	5.94	.280	97	-0.655	-1.229	-0.431	-0.791	-0.215
787.70	Mg II	10.00	.093	51	-0.472	-0.329	-0.356	-0.177	-0.202
789.63	Mg II	10.00	.131	53	-0.564	-0.418	-0.411	-0.229	-0.203
669.60	Al I	3.14	.263	99	-0.424	-1.112	-0.266	-0.876	-0.143
669.86	Al I	3.14	.156	99	-0.277	-0.993	-0.210	-0.844	-0.144
708.46	Al I	4.02	.081	97	-0.214	-1.017	-0.198	-0.776	-0.168
783.60	Al I	4.02	.287	97	-0.602	-1.200	-0.390	-0.819	-0.201
877.39	Al I	4.02	.400	93	-1.188	-1.556	-0.573	-0.855	-0.213
551.75	Si I	5.08	.119	96	-0.119	-0.829	-0.082	-0.709	-0.041
564.56	Si I	4.93	.300	99	-0.334	-1.017	-0.174	-0.784	-0.054
594.89	Si I	5.08	.577	96	-1.320	-1.680	-0.423	-0.829	-0.085
672.18	Si I	5.86	.269	96	-0.470	-1.036	-0.301	-0.733	-0.145
684.85	Si I	5.86	.114	94	-0.258	-0.868	-0.212	-0.699	-0.154
703.49	Si I	5.87	.403	96	-0.907	-1.317	-0.455	-0.779	-0.165
793.23	Si I	5.96	.454	93	-1.362	-1.651	-0.616	-0.817	-0.204
803.56	Si I	5.98	.158	95	-0.412	-0.949	-0.312	-0.743	-0.207
859.59	Si I	6.19	.226	95	-0.578	-1.058	-0.390	-0.743	-0.211
875.20	Si I	5.87	.476	91	-1.678	-1.927	-0.701	-0.848	-0.213
597.88	Si II	10.07	.043	42	-0.200	-0.062	-0.150	0.018	-0.088
634.70	Si II	8.09	.304	63	-0.755	-0.677	-0.454	-0.347	-0.119
605.26	S I	7.87	.058	66	-0.186	-0.342	-0.148	-0.208	-0.095
768.61	S I	7.87	.031	67	-0.265	-0.351	-0.234	-0.260	-0.195



$\lambda$ (nm)	Element	EP (eV)	$d$	$\Delta z_{\text{eff}}$ (km)	$I_l$	$D_l$	$\langle \log \tau_5 \rangle$ $I_l/2$ $D_l/2$		$I_c$
continued									
845.20	S I	8.04	.029	66	-0.282	-0.341	-0.249	-0.244	-0.208
869.39	S I	7.87	.064	68	-0.379	-0.427	-0.304	-0.298	-0.212
869.46	S I	7.87	.164	72	-0.629	-0.641	-0.439	-0.395	-0.212
693.87	K I	1.62	.032	97	-0.184	-0.896	-0.173	-0.806	-0.159
769.89	K I	0.00	.837	59	-5.935	-5.948	-1.141	-1.224	-0.196
450.73	Ca I	2.52	.101	101	0.060	-0.907	0.076	-0.806	0.094
451.22	Ca I	2.52	.274	103	-0.026	-1.016	0.037	-0.838	0.093
468.52	Ca I	2.93	.576	101	-0.563	-1.380	-0.115	-0.819	0.067
616.64	Ca I	2.52	.582	96	-1.495	-1.918	-0.379	-1.012	-0.105
641.76	Ca I	4.44	.090	94	-0.200	-0.841	-0.167	-0.697	-0.124
646.46	Ca I	2.52	.113	102	-0.200	-1.052	-0.164	-0.949	-0.127
657.27	Ca I	0.00	.290	115	-0.294	-1.537	-0.194	-1.333	-0.135
863.39	Ca I	4.45	.088	99	-0.275	-1.080	-0.254	-0.800	-0.212
390.00	Ca II	0.00	.117	131	0.178	-1.141	0.187	-1.055	0.197
500.14	Ca II	7.50	.117	63	-0.142	-0.305	-0.070	-0.167	0.022
533.92	Ca II	8.44	.067	60	-0.107	-0.282	-0.075	-0.120	-0.021
824.88	Ca II	7.51	.306	79	-0.979	-1.009	-0.598	-0.527	-0.204
825.47	Ca II	7.51	.095	71	-0.441	-0.501	-0.334	-0.343	-0.204
891.20	Ca II	7.05	.448	88	-1.651	-1.782	-0.799	-0.687	-0.215
985.47	Ca II	7.50	.114	73	-0.531	-0.578	-0.385	-0.381	-0.212
989.07	Na II	8.44	.232	72	-0.866	-0.837	-0.574	-0.440	-0.212
402.36	Sc I	0.02	.674	117	-0.165	-1.841	0.119	-1.283	0.175
474.38	Sc I	1.45	.076	108	0.039	-1.105	0.048	-1.037	0.058
567.18	Sc I	1.45	.110	109	-0.098	-1.192	-0.077	-1.109	-0.057
568.68	Sc I	1.44	.085	109	-0.089	-1.178	-0.074	-1.105	-0.059
623.93	Sc I	0.00	.063	115	-0.128	-1.381	-0.119	-1.321	-0.110
442.06	Sc II	0.62	.201	128	0.045	-1.148	0.078	-1.022	0.108
467.04	Sc II	1.36	.673	129	-1.100	-1.918	-0.121	-1.005	0.069
531.83	Sc II	1.36	.121	121	-0.078	-1.058	-0.047	-0.961	-0.018
552.68	Sc II	1.77	.688	124	-1.774	-2.425	-0.349	-1.025	-0.042
564.09	Sc II	1.50	.366	126	-0.409	-1.357	-0.174	-1.040	-0.054
624.56	Sc II	1.51	.302	126	-0.413	-1.339	-0.223	-1.070	-0.111
632.08	Sc II	1.50	.070	121	-0.160	-1.073	-0.139	-0.995	-0.117
401.32	Ti I	2.10	.100	106	0.156	-1.000	0.166	-0.921	0.177
406.02	Ti I	1.05	.562	115	-0.053	-1.533	0.110	-1.162	0.168
428.13	Ti I	0.81	.384	115	0.031	-1.396	0.093	-1.190	0.130
444.12	Ti I	1.87	.112	108	0.078	-1.076	0.091	-0.996	0.104
445.32	Ti I	1.43	.724	106	-1.155	-2.013	-0.015	-1.132	0.103
451.27	Ti I	0.84	.761	107	-1.619	-2.303	-0.016	-1.216	0.093
456.26	Ti I	0.02	.150	117	0.062	-1.363	0.074	-1.279	0.085
461.72	Ti I	1.75	.718	104	-1.343	-2.033	-0.065	-1.098	0.077
465.64	Ti I	0.00	.762	111	-1.749	-2.493	-0.018	-1.352	0.071
474.26	Ti I	2.24	.376	108	-0.133	-1.261	-0.013	-1.025	0.058
475.92	Ti I	2.25	.564	107	-0.504	-1.546	-0.067	-1.050	0.056
478.17	Ti I	0.85	.146	113	0.020	-1.264	0.037	-1.176	0.053
492.83	Ti I	2.15	.339	109	-0.136	-1.257	-0.033	-1.048	0.032
499.71	Ti I	0.00	.391	120	-0.103	-1.606	-0.020	-1.367	0.023
499.95	Ti I	0.83	.833	101	-3.275	-3.625	-0.141	-1.031	0.022
501.61	Ti I	0.85	.699	108	-1.489	-2.236	-0.101	-1.265	0.020
504.35	Ti I	0.84	.173	113	-0.029	-1.303	-0.005	-1.203	0.016
511.34	Ti I	1.44	.314	112	-0.124	-1.344	-0.044	-1.157	0.007
514.74	Ti I	0.00	.454	120	-0.190	-1.707	-0.052	-1.390	0.003
519.40	Ti I	2.10	.123	107	-0.047	-1.116	-0.025	-1.027	-0.003
521.03	Ti I	0.05	.784	107	-2.757	-3.190	-0.143	-1.330	-0.005

$\lambda$ (nm)	Element	EP (eV)	$d$	$\Delta z_{\text{eff}}$ (km)	$I_l$	$D_l$	$\langle \log \tau_5 \rangle$ $I_l/2$	$D_l/2$	$I_c$
continued									
521.97	Ti I	0.02	.303	119	-0.094	-1.534	-0.041	-1.359	-0.006
522.43	Ti I	2.13	.463	109	-0.397	-1.469	-0.115	-1.099	-0.007
529.57	Ti I	1.07	.138	112	-0.056	-1.268	-0.035	-1.180	-0.015
542.62	Ti I	0.02	.075	116	-0.046	-1.377	-0.039	-1.316	-0.031
549.01	Ti I	1.46	.244	111	-0.141	-1.315	-0.082	-1.165	-0.038
564.85	Ti I	2.49	.109	105	-0.104	-1.091	-0.080	-1.001	-0.055
566.21	Ti I	2.32	.233	107	-0.185	-1.214	-0.112	-1.057	-0.056
578.59	Ti I	3.32	.121	102	-0.139	-1.012	-0.105	-0.903	-0.069
589.93	Ti I	1.05	.326	114	-0.260	-1.494	-0.144	-1.268	-0.080
596.58	Ti I	1.88	.270	110	-0.249	-1.333	-0.151	-1.146	-0.087
609.11	Ti I	2.27	.148	107	-0.176	-1.178	-0.135	-1.068	-0.098
612.62	Ti I	1.07	.222	113	-0.204	-1.398	-0.145	-1.251	-0.101
625.81	Ti I	1.44	.494	110	-0.832	-1.817	-0.248	-1.270	-0.112
659.91	Ti I	0.90	.086	113	-0.169	-1.329	-0.153	-1.256	-0.137
674.31	Ti I	0.90	.158	114	-0.218	-1.395	-0.179	-1.283	-0.147
725.17	Ti I	1.43	.289	112	-0.414	-1.514	-0.259	-1.274	-0.175
836.42	Ti I	0.84	.155	115	-0.301	-1.461	-0.248	-1.333	-0.207
838.25	Ti I	0.82	.204	115	-0.350	-1.524	-0.264	-1.353	-0.207
841.23	Ti I	0.82	.272	116	-0.449	-1.628	-0.289	-1.378	-0.208
843.56	Ti I	0.84	.429	112	-1.101	-2.036	-0.359	-1.416	-0.208
439.58	Ti II	1.24	.746	129	-1.376	-2.157	-0.080	-0.983	0.112
448.83	Ti II	3.12	.584	110	-0.777	-1.316	-0.137	-0.711	0.097
449.35	Ti II	1.08	.392	128	-0.124	-1.262	0.018	-0.995	0.096
463.63	Ti II	1.16	.221	124	-0.021	-1.095	0.031	-0.955	0.074
465.72	Ti II	1.24	.585	130	-0.647	-1.639	-0.078	-1.021	0.071
471.95	Ti II	1.24	.150	121	0.001	-1.035	0.032	-0.931	0.062
487.40	Ti II	3.09	.402	108	-0.426	-1.053	-0.125	-0.728	0.040
500.51	Ti II	1.57	.248	121	-0.126	-1.100	-0.042	-0.932	0.021
506.90	Ti II	3.12	.180	103	-0.135	-0.810	-0.056	-0.680	0.013
521.15	Ti II	2.58	.377	114	-0.425	-1.146	-0.153	-0.833	-0.005
533.67	Ti II	1.57	.693	126	-1.709	-2.391	-0.297	-1.039	-0.020
539.62	Ti II	1.58	.122	119	-0.094	-1.028	-0.060	-0.931	-0.027
541.87	Ti II	1.57	.518	128	-0.797	-1.638	-0.213	-1.045	-0.030
867.53	Ti II	1.07	.146	131	-0.355	-1.335	-0.276	-1.180	-0.212
403.90	Cr I	3.85	.523	101	-0.184	-1.144	0.047	-0.742	0.172
403.93	Cr I	3.85	.090	98	0.145	-0.803	0.157	-0.689	0.172
420.44	Cr I	3.98	.208	98	0.062	-0.871	0.100	-0.707	0.143
446.07	Cr I	2.71	.161	104	0.050	-1.012	0.076	-0.903	0.101
453.51	Cr I	2.54	.433	107	-0.153	-1.273	0.007	-0.986	0.090
454.07	Cr I	3.10	.632	102	-0.763	-1.568	-0.079	-0.904	0.089
454.59	Cr I	0.94	.842	101	-2.779	-3.132	-0.040	-1.067	0.088
464.19	Cr I	3.85	.073	99	0.057	-0.985	0.062	-0.789	0.073
481.61	Cr I	4.53	.047	95	0.026	-0.773	0.035	-0.664	0.048
493.11	Cr I	5.54	.046	89	0.003	-0.647	0.015	-0.539	0.032
496.49	Cr I	0.94	.471	115	-0.224	-1.595	-0.041	-1.257	0.027
512.21	Cr I	1.03	.140	112	-0.031	-1.271	-0.012	-1.184	0.006
524.75	Cr I	0.96	.749	102	-2.349	-2.758	-0.171	-1.233	-0.010
527.19	Cr I	3.45	.269	102	-0.185	-1.097	-0.089	-0.895	-0.013
528.71	Cr I	3.44	.118	101	-0.072	-0.977	-0.044	-0.865	-0.014
529.73	Cr I	2.89	.701	94	-1.855	-2.218	-0.278	-0.972	-0.016
530.07	Cr I	0.98	.612	110	-0.974	-2.005	-0.130	-1.286	-0.016
534.83	Cr I	1.00	.784	100	-2.934	-3.281	-0.229	-1.172	-0.022
569.47	Cr I	3.86	.181	100	-0.177	-1.022	-0.118	-0.854	-0.060
578.30	Cr I	3.32	.319	103	-0.346	-1.221	-0.175	-0.965	-0.069

$\lambda$ (nm)	Element	EP (eV)	$d$	$\Delta z_{\text{eff}}$ (km)	$I_l$	$D_l$	$\langle \log \tau_5 \rangle$ $I_l/2$	$D_l/2$	$I_c$
continued									
633.01	Cr I	0.94	.267	114	-0.258	-1.486	-0.171	-1.300	-0.117
663.00	Cr I	1.03	.056	112	-0.159	-1.299	-0.149	-1.239	-0.139
666.10	Cr I	4.19	.110	99	-0.225	-0.997	-0.186	-0.852	-0.141
688.25	Cr I	3.44	.266	103	-0.444	-1.247	-0.269	-1.004	-0.156
692.60	Cr I	3.45	.157	102	-0.289	-1.115	-0.220	-0.972	-0.158
697.84	Cr I	3.46	.459	99	-1.147	-1.681	-0.403	-1.042	-0.162
735.59	Cr I	2.89	.492	99	-1.484	-1.952	-0.435	-1.131	-0.180
894.71	Cr I	3.09	.208	105	-0.480	-1.302	-0.321	-1.084	-0.215
929.04	Cr I	2.53	.352	105	-0.978	-1.704	-0.404	-1.203	-0.216
957.18	Cr I	2.53	.102	107	-0.304	-1.226	-0.257	-1.117	-0.215
458.82	Cr II	4.07	.717	105	-1.462	-1.832	-0.298	-0.646	0.081
461.66	Cr II	4.07	.495	100	-0.642	-1.067	-0.156	-0.617	0.077
523.73	Cr II	4.07	.511	103	-0.927	-1.297	-0.302	-0.705	-0.009
530.84	Cr II	4.07	.254	97	-0.324	-0.823	-0.147	-0.628	-0.017
531.06	Cr II	4.07	.134	94	-0.152	-0.689	-0.082	-0.584	-0.017
531.35	Cr II	4.07	.354	100	-0.524	-0.972	-0.209	-0.664	-0.018
550.86	Cr II	4.15	.157	95	-0.215	-0.725	-0.122	-0.601	-0.040
539.46	Mn I	0.00	.486	123	-0.275	-1.886	-0.085	-1.491	-0.027
402.24	Fe I	2.40	.321	112	0.094	-1.219	0.141	-1.050	0.175
409.15	Fe I	2.83	.765	104	-1.272	-1.988	0.035	-1.003	0.163
411.44	Fe I	2.83	.881	97	-2.762	-3.065	-0.059	-0.877	0.159
411.49	Fe I	3.37	.769	101	-1.405	-1.974	-0.005	-0.912	0.159
412.44	Fe I	3.64	.414	107	-0.039	-1.151	0.084	-0.892	0.157
419.44	Fe I	2.73	.280	110	0.065	-1.161	0.110	-1.010	0.145
423.27	Fe I	0.11	.795	118	-1.635	-2.634	0.083	-1.431	0.139
428.15	Fe I	2.45	.120	110	0.104	-1.108	0.117	-1.028	0.130
434.71	Fe I	0.00	.608	127	-0.100	-1.983	0.077	-1.489	0.119
438.92	Fe I	0.05	.835	116	-2.581	-3.146	-0.753	-2.274	0.113
443.96	Fe I	3.05	.277	109	0.005	-1.146	0.062	-0.987	0.105
443.98	Fe I	2.27	.662	111	-0.694	-1.840	0.002	-1.148	0.105
444.28	Fe I	2.17	.755	106	-1.591	-2.236	-0.018	-1.142	0.104
444.54	Fe I	0.08	.573	126	-0.095	-1.926	0.061	-1.480	0.104
447.80	Fe I	2.20	.271	113	0.022	-1.260	0.066	-1.112	0.099
448.97	Fe I	0.12	.874	111	-3.387	-3.877	0.015	-1.294	0.097
451.08	Fe I	3.60	.139	105	0.046	-0.986	0.069	-0.886	0.093
452.58	Fe I	2.88	.252	109	0.005	-1.159	0.053	-1.015	0.091
452.77	Fe I	3.25	.367	109	-0.086	-1.212	0.024	-0.985	0.091
454.64	Fe I	4.19	.086	101	0.056	-0.891	0.071	-0.796	0.088
455.16	Fe I	3.94	.354	105	-0.114	-1.120	0.007	-0.886	0.087
456.14	Fe I	2.76	.411	111	-0.112	-1.329	0.018	-1.068	0.085
457.47	Fe I	2.28	.702	108	-1.185	-2.034	-0.036	-1.151	0.083
459.35	Fe I	3.94	.340	105	-0.109	-1.111	0.004	-0.887	0.081
459.87	Fe I	3.69	.188	105	0.005	-1.015	0.044	-0.892	0.080
460.20	Fe I	1.60	.793	106	-2.215	-2.699	-0.044	-1.213	0.079
463.01	Fe I	2.28	.779	102	-2.093	-2.542	-0.078	-1.113	0.075
465.75	Fe I	2.84	.408	111	-0.139	-1.330	-0.001	-1.065	0.071
467.28	Fe I	1.61	.373	117	-0.053	-1.457	0.025	-1.238	0.069
473.35	Fe I	1.48	.818	105	-2.717	-3.132	-0.088	-1.208	0.060
474.15	Fe I	2.83	.763	100	-1.970	-2.399	-0.127	-1.046	0.058
474.51	Fe I	2.22	.162	112	0.015	-1.205	0.037	-1.109	0.058
477.60	Fe I	3.30	.304	108	-0.093	-1.177	-0.007	-0.990	0.053
478.59	Fe I	4.14	.322	104	-0.146	-1.098	-0.030	-0.875	0.052
479.05	Fe I	4.15	.104	102	0.008	-0.925	0.029	-0.827	0.051
479.39	Fe I	3.05	.097	107	0.020	-1.058	0.035	-0.980	0.051

$\lambda$ (nm)	Element	EP (eV)	$d$	$\Delta z_{\text{eff}}$ (km)	$I_l$	$D_l$	$\langle \log \tau_5 \rangle$		$I_c$
							$I_l/2$	$D_l/2$	
continued									
479.87	Fe I	1.61	.395	117	-0.098	-1.498	0.000	-1.253	0.050
480.25	Fe I	4.61	.164	100	-0.029	-0.927	0.008	-0.779	0.050
480.81	Fe I	3.25	.336	108	-0.125	-1.219	-0.019	-1.007	0.049
480.99	Fe I	3.57	.229	106	-0.055	-1.083	0.002	-0.938	0.049
487.43	Fe I	3.06	.286	109	-0.091	-1.203	-0.014	-1.029	0.040
488.54	Fe I	3.88	.722	96	-1.746	-2.139	-0.217	-0.908	0.038
490.86	Fe I	2.48	.085	110	0.011	-1.136	0.023	-1.067	0.035
491.72	Fe I	4.19	.650	99	-1.247	-1.770	-0.200	-0.894	0.034
492.47	Fe I	2.27	.808	100	-2.723	-3.077	-0.105	-0.969	0.033
496.25	Fe I	4.18	.583	102	-0.875	-1.560	-0.169	-0.914	0.027
496.99	Fe I	4.22	.715	94	-1.746	-2.112	-0.266	-0.859	0.026
498.54	Fe I	2.86	.815	97	-2.878	-3.183	-0.180	-0.872	0.024
498.62	Fe I	4.20	.535	103	-0.668	-1.443	-0.151	-0.915	0.024
499.27	Fe I	4.26	.109	101	-0.027	-0.933	-0.003	-0.831	0.023
499.54	Fe I	4.26	.162	102	-0.059	-0.971	-0.018	-0.843	0.023
501.64	Fe I	4.26	.371	104	-0.272	-1.172	-0.090	-0.890	0.020
502.96	Fe I	3.41	.564	106	-0.746	-1.613	-0.133	-1.036	0.018
504.42	Fe I	2.85	.722	101	-1.899	-2.344	-0.178	-1.082	0.016
505.46	Fe I	3.64	.445	107	-0.379	-1.350	-0.103	-0.995	0.015
505.84	Fe I	3.64	.147	105	-0.051	-1.038	-0.017	-0.931	0.014
506.71	Fe I	4.22	.671	97	-1.490	-1.922	-0.251	-0.893	0.013
507.47	Fe I	4.20	.809	89	-2.966	-3.191	-0.423	-0.754	0.012
507.97	Fe I	0.99	.825	107	-3.220	-3.65J	-0.070	-1.084	0.012
512.73	Fe I	0.91	.817	108	-3.191	-3.632	-0.073	-1.105	0.006
512.76	Fe I	0.05	.244	125	-0.043	-1.601	-0.015	-1.466	0.006
513.60	Fe I	4.19	.241	103	-0.142	-1.056	-0.062	-0.884	0.004
515.90	Fe I	4.26	.689	95	-1.684	-2.060	-0.292	-0.883	0.001
519.87	Fe I	2.22	.792	101	-2.883	-3.234	-0.233	-1.104	-0.004
522.55	Fe I	0.11	.747	117	-2.336	-2.956	-0.100	-1.499	-0.007
524.37	Fe I	4.26	.619	98	-1.282	-1.779	-0.256	-0.919	-0.009
524.70	Fe I	0.08	.716	119	-1.891	-2.711	-0.095	-1.522	-0.010
525.02	Fe I	0.12	.714	118	-1.925	-2.719	-0.097	-1.515	-0.010
525.06	Fe I	2.20	.793	101	-2.960	-3.310	-0.248	-1.102	-0.010
525.30	Fe I	2.28	.233	113	-0.100	-1.297	-0.049	-1.156	-0.010
525.34	Fe I	3.27	.725	97	-2.088	-2.454	-0.260	-1.024	-0.010
526.26	Fe I	4.32	.113	101	-0.070	-0.951	-0.042	-0.846	-0.012
526.28	Fe I	3.25	.206	107	-0.110	-1.150	-0.056	-1.016	-0.012
529.39	Fe I	4.14	.332	104	-0.278	-1.176	-0.116	-0.926	-0.015
532.00	Fe I	3.64	.220	106	-0.140	-1.119	-0.073	-0.970	-0.018
532.20	Fe I	2.28	.643	107	-1.406	-2.117	-0.167	-1.215	-0.019
535.81	Fe I	3.30	.107	106	-0.068	-1.077	-0.045	-0.991	-0.023
538.94	Fe I	4.41	.719	91	-2.116	-2.399	-0.402	-0.844	-0.026
540.67	Fe I	4.37	.388	103	-0.417	-1.243	-0.164	-0.914	-0.028
542.21	Fe I	4.32	.115	101	-0.093	-0.965	-0.063	-0.859	-0.030
543.65	Fe I	2.28	.481	113	-0.470	-1.649	-0.134	-1.223	-0.032
546.08	Fe I	3.07	.091	107	-0.071	-1.103	-0.053	-1.025	-0.035
546.15	Fe I	4.44	.272	102	-0.244	-1.096	-0.124	-0.885	-0.035
546.64	Fe I	4.35	.699	92	-2.006	-2.309	-0.390	-0.876	-0.035
548.30	Fe I	4.15	.485	103	-0.708	-1.457	-0.214	-0.966	-0.037
548.98	Fe I	4.44	.142	101	-0.123	-0.979	-0.081	-0.855	-0.038
550.14	Fe I	0.95	.816	105	-3.609	-4.032	-0.263	-1.289	-0.039
554.65	Fe I	4.37	.521	101	-0.911	-1.541	-0.257	-0.940	-0.044
554.69	Fe I	4.22	.252	103	-0.228	-1.106	-0.123	-0.917	-0.044
555.26	Fe I	4.95	.082	99	-0.092	-0.899	-0.071	-0.778	-0.045

$\lambda$ (nm)	Element	EP (eV)	$d$	$\Delta z_{\text{eff}}$ (km)	$I_l$	$D_l$	$\langle \log \tau_5 \rangle$		$I_c$
							$I_l/2$	$D_l/2$	
continued									
556.88	Fe I	3.63	.114	105	-0.103	-1.056	-0.074	-0.962	-0.046
556.96	Fe I	3.40	.811	92	-3.689	-3.940	-0.504	-0.880	-0.046
557.70	Fe I	5.03	.118	99	-0.119	-0.925	-0.087	-0.779	-0.047
563.58	Fe I	4.26	.361	104	-0.415	-1.248	-0.182	-0.945	-0.053
563.66	Fe I	3.64	.222	106	-0.191	-1.151	-0.114	-0.994	-0.053
563.82	Fe I	4.22	.669	94	-1.899	-2.230	-0.382	-0.929	-0.054
564.27	Fe I	4.61	.105	100	-0.118	-0.945	-0.087	-0.834	-0.054
565.06	Fe I	5.08	.367	100	-0.446	-1.189	-0.213	-0.827	-0.055
566.13	Fe I	4.28	.233	103	-0.228	-1.092	-0.132	-0.913	-0.056
567.90	Fe I	4.65	.556	98	-1.165	-1.660	-0.323	-0.905	-0.058
570.54	Fe I	4.30	.398	103	-0.523	-1.314	-0.211	-0.952	-0.061
572.08	Fe I	4.55	.142	101	-0.156	-0.985	-0.109	-0.857	-0.062
575.44	Fe I	3.64	.134	105	-0.138	-1.084	-0.101	-0.979	-0.066
577.84	Fe I	2.59	.233	111	-0.187	-1.303	-0.118	-1.149	-0.068
578.46	Fe I	3.40	.275	108	-0.261	-1.250	-0.145	-1.051	-0.069
580.44	Fe I	4.28	.198	103	-0.213	-1.070	-0.136	-0.914	-0.071
580.67	Fe I	4.61	.501	100	-0.950	-1.531	-0.302	-0.925	-0.071
581.48	Fe I	4.28	.236	103	-0.256	-1.110	-0.152	-0.926	-0.072
582.78	Fe I	3.28	.119	107	-0.132	-1.122	-0.102	-1.028	-0.073
584.52	Fe I	5.03	.065	98	-0.115	-0.898	-0.098	-0.784	-0.075
586.23	Fe I	4.55	.660	92	-1.961	-2.258	-0.456	-0.891	-0.077
588.12	Fe I	4.61	.146	101	-0.181	-0.995	-0.129	-0.861	-0.078
590.56	Fe I	4.65	.533	98	-1.162	-1.655	-0.346	-0.924	-0.081
591.62	Fe I	2.45	.555	109	-1.126	-1.948	-0.236	-1.237	-0.082
592.96	Fe I	4.55	.387	102	-0.567	-1.303	-0.246	-0.933	-0.083
593.01	Fe I	4.65	.669	91	-2.086	-2.358	-0.497	-0.870	-0.083
595.67	Fe I	0.85	.538	120	-0.745	-2.082	-0.181	-1.466	-0.086
598.48	Fe I	4.73	.635	92	-1.859	-2.163	-0.474	-0.882	-0.088
600.79	Fe I	4.65	.542	97	-1.258	-1.716	-0.370	-0.931	-0.090
605.60	Fe I	4.73	.609	93	-1.692	-2.028	-0.452	-0.901	-0.095
607.85	Fe I	4.79	.612	93	-1.724	-2.049	-0.467	-0.891	-0.097
608.27	Fe I	2.22	.363	114	-0.375	-1.545	-0.183	-1.253	-0.097
608.95	Fe I	5.02	.351	100	-0.535	-1.228	-0.265	-0.872	-0.098
609.43	Fe I	4.65	.189	101	-0.253	-1.048	-0.171	-0.883	-0.098
612.02	Fe I	0.91	.052	118	-0.115	-1.401	-0.108	-1.347	-0.101
613.66	Fe I	2.45	.768	97	-3.589	-3.907	-0.500	-1.064	-0.102
613.70	Fe I	2.19	.611	106	-1.748	-2.313	-0.282	-1.278	-0.102
615.93	Fe I	4.61	.116	101	-0.188	-0.989	-0.147	-0.871	-0.104
616.53	Fe I	4.14	.443	103	-0.817	-1.508	-0.295	-1.016	-0.105
621.34	Fe I	2.22	.668	103	-2.342	-2.748	-0.333	-1.248	-0.108
622.07	Fe I	3.88	.176	105	-0.234	-1.127	-0.166	-0.988	-0.109
624.06	Fe I	2.22	.488	112	-0.827	-1.838	-0.244	-1.286	-0.111
624.63	Fe I	3.60	.716	93	-2.861	-3.126	-0.536	-0.986	-0.111
625.25	Fe I	2.40	.741	99	-3.316	-3.647	-0.468	-1.119	-0.111
628.06	Fe I	0.85	.612	115	-1.759	-2.512	-0.241	-1.476	-0.114
629.39	Fe I	4.81	.114	100	-0.202	-0.976	-0.159	-0.852	-0.115
630.15	Fe I	3.65	.719	93	-3.005	-3.264	-0.573	-0.967	-0.115
631.15	Fe I	2.83	.280	111	-0.324	-1.376	-0.194	-1.163	-0.116
633.68	Fe I	3.69	.698	93	-2.779	-3.042	-0.544	-0.990	-0.118
633.88	Fe I	4.79	.396	101	-0.724	-1.365	-0.316	-0.930	-0.118
639.25	Fe I	2.28	.172	113	-0.208	-1.330	-0.161	-1.208	-0.122
641.99	Fe I	4.73	.623	91	-2.017	-2.293	-0.543	-0.910	-0.124
643.08	Fe I	2.17	.725	100	-3.247	-3.597	-0.454	-1.181	-0.125
649.89	Fe I	0.95	.442	121	-0.538	-1.907	-0.218	-1.467	-0.130

$\lambda$ (nm)	Element	EP (eV)	$d$	$\Delta z_{\text{eff}}$ (km)	$I_l$	$D_l$	$\langle \log \tau_5 \rangle$ $I_l/2$	$D_l/2$	$I_c$
continued									
657.42	Fe I	0.99	.293	121	-0.289	-1.646	-0.189	-1.428	-0.135
658.12	Fe I	1.48	.178	117	-0.213	-1.450	-0.170	-1.326	-0.135
659.38	Fe I	2.43	.646	101	-2.393	-2.774	-0.392	-1.238	-0.136
660.80	Fe I	2.28	.171	113	-0.228	-1.342	-0.177	-1.218	-0.137
662.50	Fe I	1.01	.149	119	-0.194	-1.487	-0.164	-1.383	-0.138
662.75	Fe I	4.55	.252	102	-0.410	-1.176	-0.251	-0.946	-0.139
664.69	Fe I	2.61	.094	110	-0.186	-1.233	-0.163	-1.152	-0.140
667.80	Fe I	2.69	.735	96	-3.636	-3.939	-0.611	-1.067	-0.142
669.63	Fe I	4.83	.132	100	-0.258	-1.014	-0.200	-0.877	-0.143
670.35	Fe I	2.76	.349	111	-0.508	-1.530	-0.254	-1.212	-0.144
671.03	Fe I	1.48	.145	116	-0.205	-1.426	-0.172	-1.322	-0.144
673.31	Fe I	4.64	.239	102	-0.405	-1.159	-0.255	-0.937	-0.146
673.95	Fe I	1.56	.108	116	-0.190	-1.385	-0.167	-1.300	-0.146
675.01	Fe I	2.42	.617	102	-2.188	-2.605	-0.386	-1.262	-0.147
680.42	Fe I	4.58	.130	101	-0.261	-1.042	-0.205	-0.913	-0.151
680.68	Fe I	2.73	.321	111	-0.461	-1.496	-0.252	-1.213	-0.151
682.03	Fe I	4.64	.346	102	-0.672	-1.344	-0.329	-0.971	-0.152
683.98	Fe I	2.56	.274	112	-0.372	-1.446	-0.233	-1.224	-0.153
685.51	Fe I	4.56	.556	94	-1.738	-2.074	-0.510	-0.986	-0.154
685.81	Fe I	4.61	.428	100	-1.002	-1.552	-0.392	-0.991	-0.154
686.19	Fe I	2.42	.171	112	-0.255	-1.340	-0.199	-1.211	-0.154
686.25	Fe I	4.56	.265	102	-0.469	-1.214	-0.280	-0.962	-0.154
694.52	Fe I	2.42	.627	102	-2.411	-2.791	-0.425	-1.258	-0.160
695.12	Fe I	4.56	.409	101	-0.935	-1.516	-0.383	-1.001	-0.160
697.19	Fe I	3.02	.113	109	-0.230	-1.215	-0.194	-1.117	-0.161
698.85	Fe I	2.40	.308	113	-0.442	-1.532	-0.254	-1.262	-0.162
701.03	Fe I	4.58	.109	101	-0.256	-1.032	-0.210	-0.916	-0.164
711.21	Fe I	2.99	.252	110	-0.393	-1.385	-0.254	-1.173	-0.169
712.75	Fe I	4.99	.220	100	-0.431	-1.131	-0.285	-0.906	-0.170
713.09	Fe I	4.22	.588	93	-2.144	-2.432	-0.567	-1.028	-0.170
714.25	Fe I	4.95	.291	101	-0.585	-1.246	-0.331	-0.932	-0.171
715.14	Fe I	2.48	.206	112	-0.314	-1.388	-0.230	-1.225	-0.171
718.00	Fe I	1.48	.177	117	-0.262	-1.481	-0.211	-1.350	-0.172
718.91	Fe I	3.07	.334	110	-0.584	-1.520	-0.298	-1.191	-0.173
722.86	Fe I	2.76	.233	111	-0.366	-1.394	-0.249	-1.201	-0.174
735.11	Fe I	4.99	.282	100	-0.592	-1.244	-0.341	-0.934	-0.180
735.15	Fe I	4.95	.351	100	-0.803	-1.387	-0.392	-0.956	-0.180
741.11	Fe I	4.28	.613	91	-2.555	-2.797	-0.667	-1.002	-0.183
743.05	Fe I	2.59	.121	111	-0.257	-1.294	-0.218	-1.192	-0.184
744.73	Fe I	4.95	.266	101	-0.564	-1.229	-0.336	-0.939	-0.185
744.79	Fe I	5.52	.131	98	-0.321	-1.004	-0.256	-0.822	-0.185
746.15	Fe I	2.56	.234	112	-0.379	-1.433	-0.260	-1.236	-0.185
749.50	Fe I	4.22	.661	90	-3.171	-3.395	-0.782	-0.966	-0.187
754.04	Fe I	2.73	.098	110	-0.249	-1.259	-0.218	-1.169	-0.189
754.78	Fe I	5.10	.159	100	-0.368	-1.065	-0.274	-0.888	-0.189
758.83	Fe I	5.03	.202	100	-0.443	-1.131	-0.303	-0.913	-0.191
771.90	Fe I	5.03	.217	100	-0.485	-1.161	-0.321	-0.924	-0.196
772.32	Fe I	2.27	.336	114	-0.603	-1.665	-0.310	-1.316	-0.197
774.82	Fe I	2.95	.606	98	-2.690	-3.005	-0.566	-1.196	-0.198
7J0.24	Fe I	5.08	.124	100	-0.334	-1.035	-0.266	-0.887	-0.199
780.79	Fe I	4.99	.411	97	-1.183	-1.626	-0.489	-0.979	-0.200
785.54	Fe I	5.06	.202	100	-0.467	-1.143	-0.319	-0.919	-0.201
791.28	Fe I	0.85	.384	122	-0.649	-1.963	-0.302	-1.524	-0.203
793.71	Fe I	4.31	.639	90	-3.227	-3.445	-0.830	-0.978	-0.204

$\lambda$ (nm)	Element	EP (eV)	$d$	$\Delta z_{\text{eff}}$ (km)	$I_l$	$D_l$	$\langle \log \tau_5 \rangle$ $I_l/2$	$D_l/2$	$I_c$
continued									
749.50	Fe I	4.22	.661	90	-3.171	-3.395	-0.782	-0.966	-0.187
795.91	Fe I	5.03	.166	100	-0.407	-1.100	-0.299	-0.914	-0.205
804.76	Fe I	0.86	.455	119	-1.129	-2.223	-0.335	-1.540	-0.208
807.50	Fe I	0.91	.281	122	-0.421	-1.748	-0.278	-1.490	-0.209
811.21	Fe I	2.69	.121	111	-0.293	-1.305	-0.248	-1.198	-0.210
829.35	Fe I	3.30	.413	105	-1.203	-1.841	-0.419	-1.207	-0.205
823.91	Fe I	2.42	.357	113	-0.769	-1.741	-0.344	-1.310	-0.204
832.70	Fe I	2.19	.676	9 7	-3.973	-4.293	-0.760	-1.191	-0.206
840.14	Fe I	2.48	.225	113	-0.420	-1.471	-0.288	-1.264	-0.207
842.58	Fe I	1.01	.046	118	-0.227	-1.450	-0.218	-1.393	-0.208
843.95	Fe I	4.55	.464	95	-1.645	-1.999	-0.561	-1.044	-0.208
851.51	Fe I	3.02	.521	100	-2.107	-2.487	-0.514	-1.237	-0.210
860.70	Fe I	5.01	.131	100	-0.372	-1.067	-0.289	-0.908	-0.211
861.18	Fe I	2.84	.577	99	-2.746	-3.064	-0.596	-1.224	-0.211
861.39	Fe I	4.99	.214	101	-0.538	-1.195	-0.349	-0.943	-0.211
861.62	Fe I	4.91	.304	101	-0.814	-1.390	-0.422	-0.983	-0.211
868.86	Fe I	2.17	.697	92	-4.561	-4.826	-0.895	-1.186	-0.212
869.94	Fe I	4.95	.422	96	-1.423	-1.797	-0.553	-0.997	-0.212
901.39	Fe I	2.28	.180	114	-0.368	-1.449	-0.278	-1.283	-0.215
936.23	Fe I	2.28	.375	112	-1.033	-1.913	-0.380	-1.351	-0.216
449.14	Fe II	2.85	.749	115	-1.594	-2.097	-0.238	-0.733	0.096
462.05	Fe II	2.83	.587	114	-0.887	-1.420	-0.167	-0.752	0.077
465.69	Fe II	2.89	.410	109	-0.392	-1.034	-0.088	-0.713	0.071
467.01	Fe II	2.57	.355	111	-0.265	-1.000	-0.054	-0.745	0.069
483.31	Fe II	2.66	.122	105	-0.036	-0.773	0.006	-0.682	0.045
499.33	Fe II	2.81	.423	111	-0.528	-1.144	-0.157	-0.769	0.023
513.26	Fe II	2.81	.271	108	-0.265	-0.939	-0.106	-0.739	0.005
523.46	Fe II	3.22	.722	112	-1.978	-2.453	-0.449	-0.791	-0.008
526.48	Fe II	3.22	.485	110	-0.834	-1.304	-0.266	-0.765	-0.012
541.39	Fe II	3.22	.290	105	-0.388	-0.956	-0.172	-0.719	-0.029
553.48	Fe II	3.24	.572	112	-1.266	-1.703	-0.384	-0.814	-0.043
599.13	Fe II	3.15	.295	108	-0.515	-1.061	-0.254	-0.786	-0.089
608.39	Fe II	3.20	.203	105	-0.352	-0.925	-0.208	-0.750	-0.097
623.83	Fe II	3.87	.365	104	-0.796	-1.167	-0.367	-0.749	-0.110
638.37	Fe II	5.55	.089	81	-0.278	-0.536	-0.200	-0.434	-0.121
644.29	Fe II	5.55	.035	79	-0.185	-0.463	-0.156	-0.403	-0.126
644.64	Fe II	6.22	.037	73	-0.196	-0.397	-0.163	-0.333	-0.126
645.63	Fe II	3.90	.524	107	-1.423	-1.786	-0.541	-0.826	-0.127
648.21	Fe II	6.22	.058	74	-0.241	-0.432	-0.187	-0.351	-0.128
651.60	Fe II	2.89	.456	116	-1.111	-1.599	-0.427	-0.924	-0.131
722.23	Fe II	3.89	.155	100	-0.429	-0.873	-0.291	-0.711	-0.174
751.58	Fe II	3.90	.112	99	-0.366	-0.823	-0.273	-0.700	-0.188
771.17	Fe II	3.90	.347	106	-1.011	-1.360	-0.502	-0.840	-0.196
402.76	Ni I	3.90	.576	105	-0.266	-1.282	0.044	-0.802	0.174
441.05	Ni I	3.31	.616	107	-0.634	-1.547	-0.032	-0.945	0.109
447.04	Ni I	3.40	.794	97	-2.032	-2.398	-0.148	-0.851	0.100
451.99	Ni I	1.68	.474	117	-0.125	-1.514	0.029	-1.191	0.092
470.59	Ni I	3.64	.143	103	0.005	-0.964	0.034	-0.857	0.064
473.24	Ni I	4.10	.505	104	-0.458	-1.302	-0.094	-0.854	0.060
479.09	Ni I	1.95	.160	113	0.007	-1.206	0.030	-1.108	0.051
481.19	Ni I	3.66	.252	105	-0.083	-1.055	-0.010	-0.889	0.048
481.59	Ni I	3.54	.180	105	-0.033	-1.013	0.009	-0.889	0.048
490.44	Ni I	3.54	.767	96	-2.134	-2.472	-0.256	-0.878	0.035
493.58	Ni I	3.94	.632	101	-1.165	-1.716	-0.195	-0.893	0.031

$\lambda$ (nm)	Element	EP (eV)	$d$	$\Delta z_{\text{eff}}$ (km)	$I_l$	$D_l$	$\langle \log \tau_5 \rangle$ $I_l/2$	$D_l/2$	$I_c$
continued									
496.75	Ni I	3.80	.164	103	-0.054	-0.985	-0.013	-0.863	0.027
497.63	Ni I	1.68	.464	117	-0.256	-1.583	-0.050	-1.230	0.025
500.37	Ni I	1.68	.403	117	-0.175	-1.493	-0.042	-1.220	0.022
503.27	Ni I	3.90	.243	104	-0.126	-1.044	-0.047	-0.874	0.018
508.41	Ni I	3.68	.758	94	-2.284	-2.593	-0.322	-0.861	0.011
509.44	Ni I	3.83	.358	105	-0.270	-1.182	-0.094	-0.914	0.010
515.79	Ni I	3.61	.220	105	-0.122	-1.071	-0.054	-0.919	0.002
517.65	Ni I	3.88	.595	102	-1.108	-1.685	-0.220	-0.932	-0.001
538.83	Ni I	1.93	.148	113	-0.077	-1.249	-0.051	-1.152	-0.026
543.58	Ni I	1.99	.546	114	-0.753	-1.818	-0.154	-1.230	-0.032
546.81	Ni I	3.85	.140	103	-0.115	-1.005	-0.075	-0.891	-0.035
549.48	Ni I	4.10	.207	103	-0.179	-1.037	-0.103	-0.877	-0.038
557.87	Ni I	1.68	.551	115	-0.823	-1.910	-0.167	-1.285	-0.047
558.93	Ni I	3.90	.290	104	-0.286	-1.156	-0.143	-0.932	-0.048
562.53	Ni I	4.09	.402	104	-0.523	-1.301	-0.205	-0.933	-0.052
562.83	Ni I	4.09	.153	102	-0.151	-1.002	-0.100	-0.874	-0.053
563.87	Ni I	3.90	.096	102	-0.107	-0.978	-0.081	-0.885	-0.054
564.30	Ni I	4.16	.160	102	-0.160	-1.002	-0.105	-0.867	-0.054
574.83	Ni I	1.68	.294	117	-0.215	-1.449	-0.121	-1.249	-0.065
575.46	Ni I	1.93	.646	108	-1.810	-2.369	-0.241	-1.244	-0.066
580.52	Ni I	4.17	.393	103	-0.555	-1.306	-0.229	-0.935	-0.071
584.70	Ni I	1.68	.226	116	-0.176	-1.385	-0.118	-1.236	-0.075
599.67	Ni I	4.23	.188	102	-0.237	-1.049	-0.158	-0.891	-0.089
600.73	Ni I	1.68	.266	116	-0.231	-1.442	-0.145	-1.257	-0.090
608.62	Ni I	4.26	.395	103	-0.652	-1.349	-0.274	-0.945	-0.098
610.81	Ni I	1.68	.592	111	-1.544	-2.244	-0.259	-1.312	-0.100
611.97	Ni I	4.26	.107	101	-0.178	-0.981	-0.139	-0.872	-0.101
617.67	Ni I	4.09	.533	100	-1.306	-1.776	-0.373	-0.982	-0.106
617.72	Ni I	1.83	.146	114	-0.169	-1.315	-0.135	-1.211	-0.106
632.21	Ni I	4.15	.158	102	-0.243	-1.053	-0.176	-0.913	-0.117
632.76	Ni I	1.68	.360	117	-0.405	-1.607	-0.203	-1.301	-0.117
648.28	Ni I	1.98	.363	116	-0.465	-1.594	-0.227	-1.270	-0.128
653.28	Ni I	1.93	.149	114	-0.206	-1.326	-0.166	-1.216	-0.132
659.86	Ni I	4.23	.214	103	-0.347	-1.126	-0.228	-0.935	-0.137
676.77	Ni I	1.83	.633	106	-2.373	-2.813	-0.385	-1.295	-0.148
677.23	Ni I	3.66	.424	105	-0.925	-1.592	-0.346	-1.072	-0.149
684.20	Ni I	3.66	.224	106	-0.369	-1.218	-0.242	-1.025	-0.153
691.45	Ni I	1.95	.554	109	-1.730	-2.314	-0.354	-1.313	-0.158
700.15	Ni I	1.93	.104	114	-0.215	-1.308	-0.188	-1.221	-0.163
711.09	Ni I	1.93	.295	116	-0.427	-1.547	-0.255	-1.288	-0.169
712.22	Ni I	3.54	.639	95	-2.666	-2.952	-0.620	-1.040	-0.170
738.52	Ni I	2.74	.381	111	-0.799	-1.662	-0.336	-1.215	-0.182
740.11	Ni I	5.36	.111	98	-0.292	-0.974	-0.243	-0.796	-0.183
742.22	Ni I	3.63	.595	96	-2.371	-2.674	-0.597	-1.068	-0.181
748.14	Ni I	5.49	.080	97	-0.258	-0.952	-0.228	-0.777	-0.186
755.56	Ni I	3.85	.585	95	-2.326	-2.619	-0.620	-1.047	-0.190
757.40	Ni I	3.83	.472	100	-1.460	-1.909	-0.473	-1.086	-0.190
786.37	Ni I	4.54	.106	101	-0.311	-1.037	-0.256	-0.911	-0.202
771.55	Ni I	3.70	.361	105	-0.870	-1.549	-0.386	-1.098	-0.196
877.06	Ni I	2.74	.094	110	-0.287	-1.245	-0.249	-1.147	-0.213
896.81	Ni I	5.32	.142	99	-0.414	-1.041	-0.314	-0.839	-0.215
472.21	Zn I	4.03	.696	104	-1.505	-1.917	-0.193	-0.824	0.061
636.23	Zn I	5.79	.192	91	-0.380	-0.857	-0.236	-0.682	-0.120
460.73	Sr I	0.00	.603	111	-0.610	-1.831	-0.017	-1.210	0.078



$\lambda$ (nm)	Element	EP (eV)	$d$	$\Delta z_{\text{eff}}$ (km)	$I_l$	$D_l$	$\langle \log \tau_5 \rangle$ $I_l/2$ $D_l/2$		$I_c$
continued									
366.37	Zr I	0.15	.341	119	0.192	-1.430	0.220	-1.262	0.240
468.78	Zr I	0.73	.136	114	0.037	-1.297	0.052	-1.214	0.066
473.94	Zr I	0.65	.076	114	0.044	-1.274	0.051	-1.215	0.059
405.03	Zr II	0.71	.367	132	0.018	-1.283	0.116	-1.041	0.170
408.57	Zr II	0.93	.071	123	0.145	-0.996	0.154	-0.932	0.164
420.89	Zr II	0.71	.622	137	-0.596	-1.822	0.027	-1.107	0.143
511.22	Zr II	1.66	.106	119	-0.050	-1.006	-0.020	-0.919	0.007
852.50	Zr II	2.41	.082	117	-0.313	-1.066	-0.260	-0.964	-0.210
455.40	Ba II	0.00	.940	89	-5.552	-5.757	-0.208	-0.919	0.087
585.36	Ba II	0.60	.650	134	-2.117	-2.935	-0.311	-1.279	-0.076
649.69	Ba II	0.60	.781	115	-4.352	-4.915	-0.684	-1.133	-0.129
447.93	Ce II	0.56	.253	135	0.002	-1.322	0.059	-1.149	0.098
452.30	Ce II	0.52	.175	134	0.034	-1.258	0.065	-1.139	0.091
456.23	Ce II	0.48	.296	138	-0.041	-1.398	0.038	-1.185	0.085
477.39	Ce II	0.92	.111	129	0.012	-1.158	0.034	-1.071	0.054
527.42	Ce II	1.04	.098	128	-0.058	-1.175	-0.035	1.090	-0.013
402.13	Nd II	0.32	.227	136	0.120	-1.293	0.151	-1.156	0.175
405.99	Nd II	0.20	.124	135	0.143	-1.238	0.156	-1.157	0.168
415.60	Nd II	0.18	.382	142	0.016	-1.513	0.106	-1.236	0.152
525.55	Nd II	0.20	.092	137	-0.042	-1.333	-0.026	-1.253	-0.011
446.73	Sm II	0.66	.137	130	0.057	-1.191	0.080	-1.096	0.100
452.39	Sm II	0.43	.124	133	0.055	-1.229	0.074	-1.140	0.091
407.31	Dy II	0.54	.120	127	0.134	-1.101	0.150	-1.025	0.166
368.34	Pb I	0.97	.165	115	0.211	-1.232	0.224	-1.149	0.236